Nanoscale Research Letters

NANO EXPRESS Open Access

Co-dosing Ozone and Deionized Water as Oxidant Precursors of ZnO Thin Film Growth by Atomic Layer Deposition

Yung-Chen Cheng[1*], Hsiang-Chen Wang[2], Shih-Wei Feng[3], Tsai-Pei Li[1], Siu-Keung Fung[3], Kai-Yun Yuan[4] and Miin-Jang Chen[4*]

Abstract

Characteristics of atomic layer deposition (ALD)-grown ZnO thin films on sapphire substrates with and without three-pulsed ozone (O_3) as oxidant precursor and post-deposition thermal annealing (TA) are investigated. Deposition temperature and thickness of ZnO epilayers are 180 °C and 85 nm, respectively. Post-deposition thermal annealing is conducted at 300 °C in the ambience of oxygen (O_2) for 1 h. With strong oxidizing agent O_3 and post-deposition TA in growing ZnO, intrinsic strain and stress are reduced to 0.49% and 2.22 GPa, respectively, with extremely low background electron concentration (9.4×10^{15} cm^{-3}). This is originated from a lower density of thermally activated defects in the analyses of thermal quenching of the integrated intensity of photoluminescence (PL) spectra. TA further facilitates recrystallization forming more defect-free grains and then reduces strain and stress state causing a remarkable decrease of electron concentration and melioration of surface roughness.

Keywords: Zinc oxide, Atomic layer deposition, Strain relaxation, Ozone precursor, Thermal annealing, Photoluminescence

Introduction

Several oxidizing agents are used in the growth of ZnO. They include water (H_2O), hydrogen peroxide (H_2O_2), oxygen (O_2), and ozone (O_3) [1–6]. H_2O is a commonly used oxidant in the growth of ZnO with atomic layer deposition (ALD). ALD is a layer-by-layer self-limiting growth mechanism. Specific surface ligands exchange reactions with sequential pulsing of respective precursors. Surface reactions stop and saturate when the reactive sites of the surface are completely depleted. ALD growth of thin films has advantages such as superior conformal deposition on surfaces and side regions, excellent step coverages of edges, high uniformity over a large area, precision in layer thickness control, and suitable for low deposition temperature [7–9].

Strong oxidizing agents influence not only the material structures but optoelectrical characteristics of ALD-deposited ZnO. H_2O_2 oxidant provides more oxygen-rich conditions than commonly used H_2O precursor to passivate defects oxygen vacancies (V_O) and zinc interstitials (Zn_i) in ALD-grown ZnO films at low growth temperatures from 80 to 150 °C. Columnar surface morphologies with (002) preferential orientation of growth plane occurred when the use of oxidant is altered from H_2O to H_2O_2 [2]. H_2O_2 oxidant increases the growth rates by approximately 70% as compared with using O_3 gas reactant of ALD-grown ZnO at 200 °C. Rise of hydroxyl (OH) group density on the growing surface of the films is responsible for the increase of growth rates [3]. The increase of growth rate of ZnO about 60% for using pure O_2 instead of H_2O as an oxidizer is reported, too [4].

* Correspondence: chengyc@mail.nutn.edu.tw; mjchen@ntu.edu.tw
[1]Department of Materials Science, National University of Tainan, Tainan 70005, Taiwan
[4]Department of Materials Science and Engineering, National Taiwan University, Taipei 10617, Taiwan
Full list of author information is available at the end of the article

O_3 is an effective oxidizer in ALD-grown oxide materials. The high electrochemical potential of O_3 gives rise to fast reaction rates at a low growth temperature. O_3 is more volatile than H_2O, H_2O_2, and O_2, and it is easier to purge. Therefore, purge times in each cycle can be shortened. The absence of hydrogen in O_3 molecule leads to less hydrogen and hydroxyl contamination in the growth. Less uniform in thickness due to recombinative surface loss of ZnO is shown for 10 s of O_3 exposure times when the growth is at 200 °C [5]. ALD-prepared undoped ZnO films with O_3 oxidizing agents show a double thermoelectric power factor compared to samples with H_2O oxidizer. H_2O- and O_3-grown ZnO films have the same defect levels of V_O but different Zn-related defect levels. Sufficient oxidation power of the O_3 results in a lower content of native Zn_i and hence a larger thermoelectric power factor. Strong oxidant effect of O_3 elevates the thermoelectric performance of undoped ZnO films [6]. Co-dosing O_3 and H_2O could improve the uniformity and conformality of ZnO thin film for proper ALD processes [5].

Intrinsic and extrinsic strains exist in ZnO film grown on a sapphire substrate naturally. Intrinsic strain is originated from high-density crystallographic imperfections in ZnO. Crystallographic imperfections include hydrogen complexes, zinc interstitials (Zn_i), oxygen vacancies (V_O), threading dislocations (TDs), and grain boundaries (GBs) [10–21]. Extrinsic strain is generated from a large mismatch of lattice constants and thermal expansion coefficients between ZnO epilayer and sapphire substrate. Various manners are exerted to diminish the intrinsic and extrinsic strain of ZnO materials on sapphires. Thin MgO buffer layer can diminish extrinsic strain, reduce surface roughness by 58.8%, and suppress surface cracks of ZnO thin film on sapphire [22]. Extrinsic strain of ZnO on sapphire is fully relaxed with the thickness reaching 30 nm prepared by magnetron sputter deposition at 550 °C [23]. Relaxation of compressive stress from 1.77 to 1.47 GPa of ZnO films deposited by spray pyrolysis method with the rise of glass substrate temperatures from 350 to 450 °C is exhibited [24].

ALD ZnO grown at 180 °C with one-pulsed precursors (DEZn and H_2O) shows background electron concentration as high as $\sim 10^{18}\,cm^{-3}$ even with post-deposition TA [25]. Commonly used one-pulsed H_2O precursors of ALD processes do not generate ideal monolayer of oxygen atoms. Three-pulsed precursors (DEZn and H_2O) could generate multiple hits or collisions of precursor molecules with surface ligand to promote the reaction probability for the ALD ZnO grown at low temperature 100 °C. The choice of "three" pulses helps securing of reactants locating the open chemisorption or reaction site properly. Extremely low background electron concentration $8.4 \times 10^{14}\,cm^{-3}$, high electron drift mobility $62.1\,cm^2/Vs$, and pronounced enhancement of near bandgap edge (NBE) photoluminescence (PL) of three-pulsed precursors ZnO with suitable buffer layer and RTA conditions are acquired [26]. Several reports show enhancement of material quality of ZnO thin films and ZnO/ZnMgO multiple quantum wells with thermal annealing [27, 28]. In this report, three-pulsed O_3 and subsequent one-pulsed H_2O as oxidizers per ALD cycle are used to grow ZnO thin films at 180 °C. Post-deposition thermal annealing (TA) is applied to improve crystalline quality of the samples. Material micro- and nano-structural, photoluminescence, and Hall effect features of ALD-grown ZnO thin films are explored.

Experimental Methods

ZnO epilayers are deposited on conventional c-face sapphire (c-Al_2O_3) substrates by Cambridge Nano-Tech Savannah 100 ALD system. In the growth of ALD ZnO thin films, precursors including deionized (DI) H_2O, O_3, and diethyl zinc (DEZn, $Zn(C_2H_5)_2$) are utilized. Table 1 demonstrates conditions of pulse number of O_3 and post-deposition TA of three specimens named A, B, and C. A schematic diagram of pulse sequence with time per ALD cycle of samples is displayed in Fig. 1. In this figure, one ALD cycle contains six sequential steps. The first step is the injection of one-pulsed deionized (DI) H_2O into a meter-scale reactor to make hydroxyl (OH)-terminated surface on sapphire or to react with the dangling ethyl groups (C_2H_5) forming zinc-oxygen (Zn–O) bridges on Zn surface with hydroxyl surface groups. One atomic layer of oxygen (O) is produced. The second step is the purge of high purity nitrogen gas (N_2) to remove excess precursor molecules and volatile byproducts and to prevent mixing of subsequent precursors after each exposure of reactants. The third step is the injection of three-pulsed O_3 into reactors to facilitate the reduction of native defects. The fourth step is the purge of the chamber by N_2

Table 1 Pulse number of ozone, thermal annealing, strain, and stress of specimens

Sample	Pulse number of ozone	Thermal annealing	Strain (%)	Stress (GPa)
A	0	No	1.08	4.90
B	3	No	0.74	3.37
C	3	300 °C, 1 h, O_2	0.49	2.22

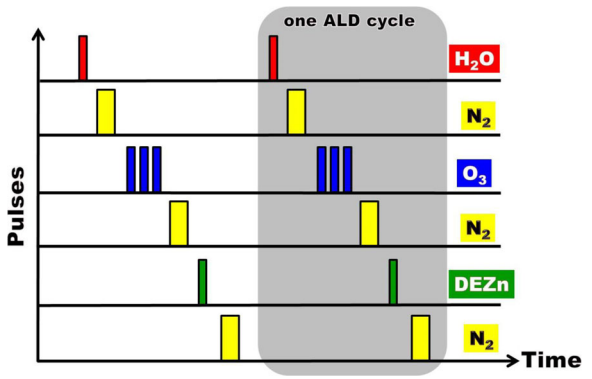

Fig. 1 ALD-grown ZnO films on sapphire substrates with pulse sequence $H_2O/N_2/O_3/N_2/DEZn/N_2$ using DI water, O_3, and $Zn(C_2H_5)_2$ as the precursors

gas. The fifth step is the injection of one-pulsed DEZn into reactors to produce one atomic layer of zinc (Zn) upon the oxygen layer. The final step is also the purge of the chamber by N_2 gas. Precursors pulsed into the reaction chamber through carry gas N_2 with a chamber pressure of 4×10^{-1} Torr. The optimal condition of exposure time for the reactants DI H_2O, O_3, and DEZn is 0.01, 0.5, and 0.015 s, respectively. The pulse time of the evacuation of the chamber is 5 s. The thickness of ZnO thin films is 85 nm with 500 ALD cycles of each sample. Other favorable conditions of deposition parameters are shown in the previous reports [29]. Post-deposition TA at 300 °C in the ambience of O_2 for 1 h in a furnace is processed on sample C.

Material structural, optical, and electrical properties of samples are conducted by the following measurements. The X-ray diffraction (XRD) patterns are measured with diffraction angle (2θ) range from 33 to 38° and wavelength 0.154 nm of copper Kα radiation by using the instrument D2 phaser (Bruker Corporation). Hall effect measurement uses Ecopia HMS-3000 system, and specimens are cut into squares having a size area of $0.7 \times 0.7\ cm^2$. Four corners of the specimens are soldered by small indium blobs showing ohmic contacts in van der Pauw configuration. Sheet carrier density, mobility, and resistivity of the films are measured. Photoluminescence (PL) spectra are carried out from 10 to 300 K with an excitation wavelength of 325 nm and a power of 55 mW of He–Cd laser. Thermal quenching of integrated intensity of PL spectra with the increase of temperature is analyzed. Surface texture and roughness of specimens examined from high-resolution images of atomic force microscope (AFM) are taken by the instrument of Veeco Dimension 3100.

Results and Discussion

Figure 2 demonstrates the crystalline nature of the specimens by the measurements of XRD patterns. Two Bragg diffraction peaks (002) and (101) correspond to the hexagonal wurtzite structure of ZnO. The strongest peak intensity of XRD patterns is normalized for comparison of peak intensity among samples. Two green arrows indicated on the top horizontal axis show diffraction angles 34.4° and 36.2° of (002) and (101), respectively, of strain-free bulk ZnO acquired from the material data sets released by the organization of Joint Committee on Powder Diffraction Standards (JCPDS). In the figure, one can observe the (002) and (101) peaks in sample B and C approach and further approach diffraction angles of (002) and (101) of strain-free bulk ZnO.

Biaxial strain along the c-axis of the epitaxial layers can be obtained through the shift of XRD patterns along (002) in contrast with strain-free bulk ZnO. Average strain (ε_z) in the lattice of ZnO films is estimated from the lattice parameters using the following expression.

$$\varepsilon_z = \frac{c - c_0}{c_0} \times 100\% \quad (1)$$

where c and c_0 are the lattice constants along the c-axis calculated from Bragg's diffraction angles of (002) peaks of ZnO films and bulk. The average stress (σ) in the plane of the films can be calculated using the biaxial strain model:

$$\sigma = \frac{2c_{13}^2 - c_{33}(c_{11}+c_{12})}{c_{13}} \times \varepsilon_z = -453.6 \times \varepsilon_z (\mathrm{GPa}) \quad (2)$$

where c_{11} = 209.7 GPa, c_{12} = 121.1 GPa, c_{13} = 105.1 GPa, and c_{33} = 210.9 GPa are the elastic stiffness constants of

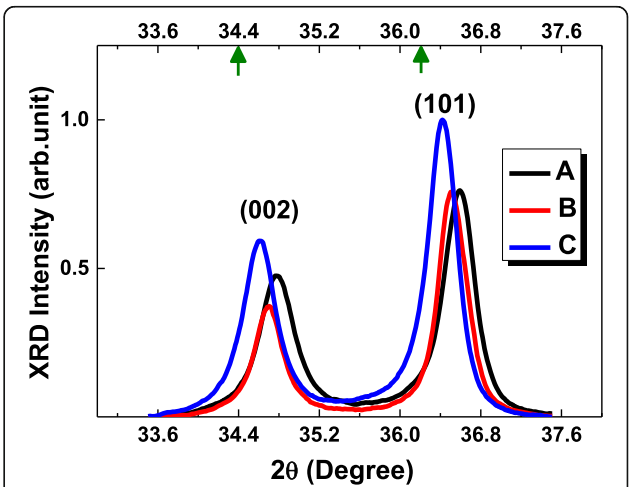

Fig. 2 XRD patterns of ZnO films with crystalline orientations along (002) and (101) directions of the specimens. The arrows indicate the diffraction angles 34.4° and 36.2° of (002) and (101) of bulk ZnO, respectively

bulk ZnO. In Table 1, the strains/stresses (ε_z/σ) of A, B, and C samples are 1.08%/4.90 GPa, 0.74%/3.37 GPa, and 0.49%/2.22 GPa, respectively. Strain/stress is reduced and further reduced in samples B and C.

PL spectra at various temperatures from 10 to 300 K of samples are displayed in Fig. 3. Strong near band edge radiative recombination of excitons with spectral peak energy around 3.34 eV is dominant in PL spectra of all samples. Longitudinal-optical (LO) phonon-assisted optical emission is observed at the lower energy shoulder of the PL spectra of samples. In Fig. 4a–c, it exhibits the Arrhenius plot of integrated intensity of PL spectra versus the inverse of temperature. Thermal quenching of integrated intensity of PL with increasing temperature can be fitted by the following Arrhenius formula.

$$I(T) = \frac{A}{1 + D_{nr1}\exp\left(\frac{-E_{A1}}{k_B T}\right) + D_{nr2}\exp\left(\frac{-E_{A2}}{k_B T}\right)} \quad (3)$$

where $I(T)$ represents the integrated PL intensity. A is a constant. D_{nr1} and D_{nr2} are constants related to the density of non-radiative recombination centers. E_{A1} and E_{A2} are the activation energies corresponding to the non-radiative recombination process of donor bound excitons at low temperature and free excitons at high temperature, respectively. k_B is the Boltzmann constant. Least squares method in regression analysis is utilized to fit the data showing the parameters of D_{nr1}, D_{nr2}, E_{A1}, and E_{A2} with red fitting curves in Table 2 and Fig. 4a–c. The fitting result shows that variations of D_{nr1}, E_{A1}, and E_{A2} among samples are light. D_{nr2} are 132.7, 153.6, and 110.8 of samples A, B, and C, respectively, showing a large difference in the amount of defect density. The smallest value of D_{nr2} suggests the lowest density of thermally activated defects in sample C.

Background electron concentration, mobility, and resistivity of Hall effect measurements of samples are listed in Table 2. In sample B, two orders of magnitude decrease of carrier concentration with reduction of mobility are shown as compared with sample A. Further immense decrease of carrier concentration to the lowest value of $9.4 \times 10^{15}\,\mathrm{cm}^{-3}$ and the rise of mobility to a value $6.1\,\mathrm{cm}^2/\mathrm{Vs}$ are observed in sample C as compared with sample B. The least amount of electron concentration is due to the largest relaxation of strain/stress states

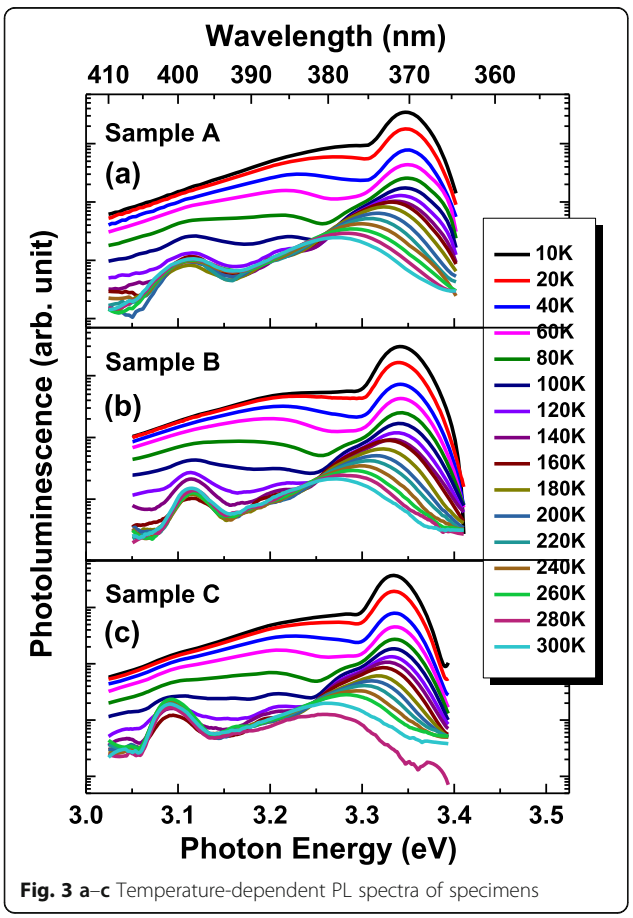

Fig. 3 a–c Temperature-dependent PL spectra of specimens

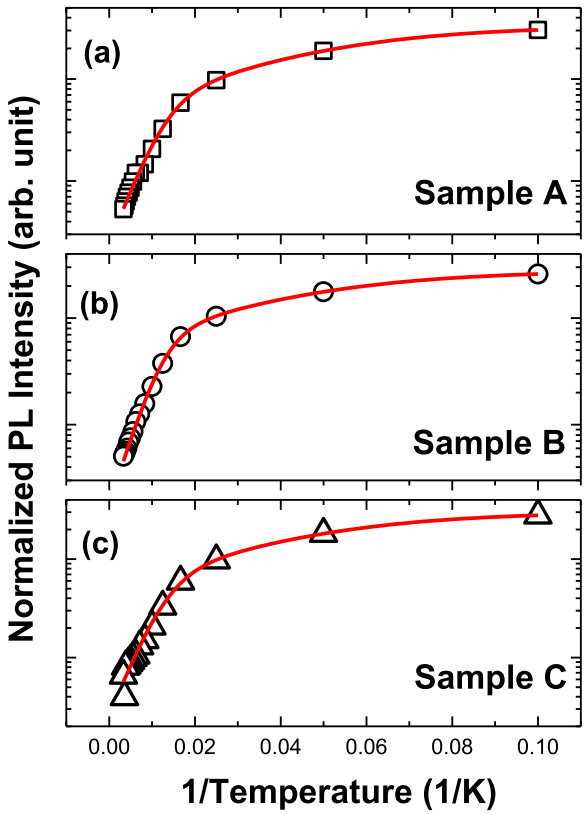

Fig. 4 a–c Arrhenius plots of thermal quenching of integrated intensity of PL spectra and red fitting curves of samples

Table 2 Carrier concentration, mobility, and resistivity of Hall effect measurements and root mean square (rms) surface roughness estimated by AFM images of specimens

Sample	Carrier concentration (cm^{-3})	Mobility (cm^2/Vs)	Resistivity (Ωcm)	D_{nr1}	E_{A1} (meV)	D_{nr2}	E_{A2} (meV)	Roughness (nm)
A	3.4×10^{19}	19	9.7×10^{-3}	6.26	3.6	132.7	22.3	1.92
B	4.6×10^{17}	1.1	1.2×10^{1}	4.3	3.4	153.6	25.6	4.30
C	9.4×10^{15}	6.1	1.1×10^{2}	5.29	3.5	110.8	21.7	2.18

and remarkable reduction of native defect density in sample C.

Figures 5a–c and d–f are 2D and 3D AFM images of specimens. Root mean square (RMS) roughness of A, B, and C is 1.92, 4.30, and 2.18 nm, respectively, as shown in Table 2. The lowest surface texture roughness occurred in sample A. With the use of O_3 precursor in sample B, surface roughness is increased. Reduction of spatial uniformity of the ALD ZnO films is due to the surface loss of O_3 [21]. Surface loss of O_3 is related to the transition from reaction- to recombination-limited growth and can constitute the primary atomic loss channel to destroy the films resulting in poor thickness uniformity. This is correlated to the reduction of diffraction peak intensity along (002) in sample B in Fig. 2. With the treatment of post-deposition TA in sample C, surface uniformity is meliorated. Meanwhile, a dramatic decrease of background electron concentration and increase of mobility are achieved. Thermal annealing brings about migration in crystal lattice; thus, metallurgic recrystallization takes place. Recrystallization accompanies the reduction in strength of strain/stress and intrinsic crystal lattice imperfections; therefore, better quality of ZnO thin film is attained. This result is consistent with the enhancement of two diffraction peak intensities in XRD pattern in sample C. It is worthy to note that electrons' mobility can be affected by scattering sources such as impurities, lattices, and defects. That scattering sources could alter the average electron velocity. In general, reduction of defect density and hence decrease of electron concentration lead to the rise of mobility. In this report, an increase of roughness of surface texture due to the action of dosing ozone precursor could cause lower electron mobility in sample C than A. In Fig. 6, a pyramid diagram containing three triangles in different colors illustrates the three key growing and processing conditions to achieve high-quality ALD ZnO epilayers in this report.

Conclusions

One-pulsed H_2O and three-pulsed strong oxidant O_3 precursors in the ALD processes can diminish the strain/stress and hence conspicuously reduce electron concentration in ZnO thin film but increase surface

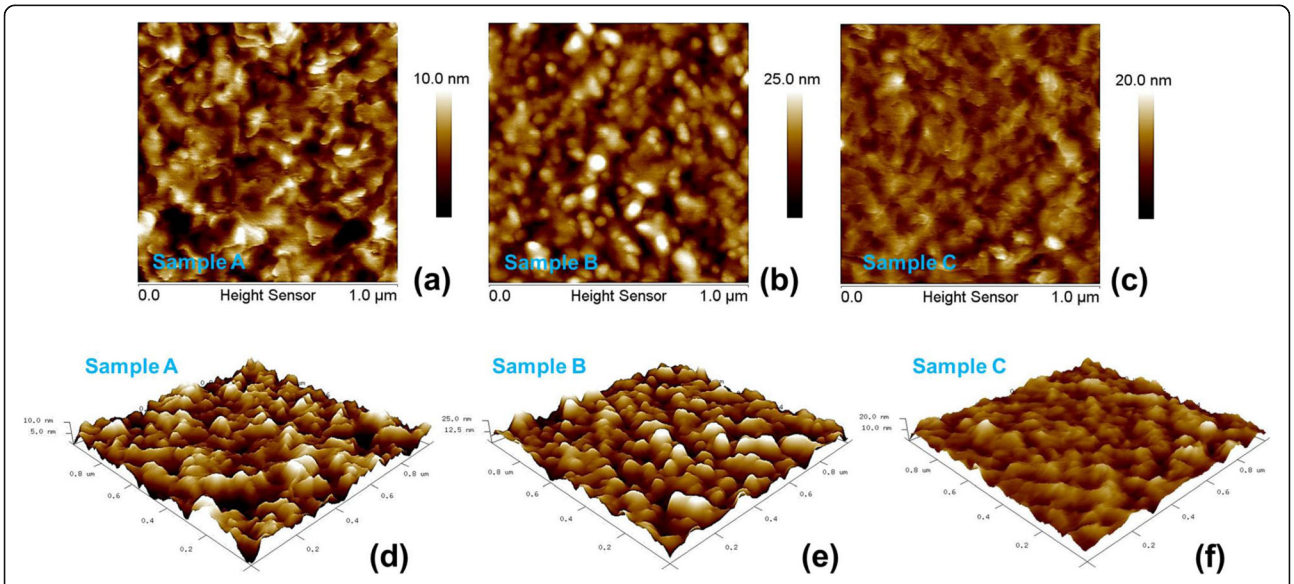

Fig. 5 **a**–**c** 2D and **d**–**f** 3D AFM images of specimens. The scale of height in 2D images are presented on the right color bar

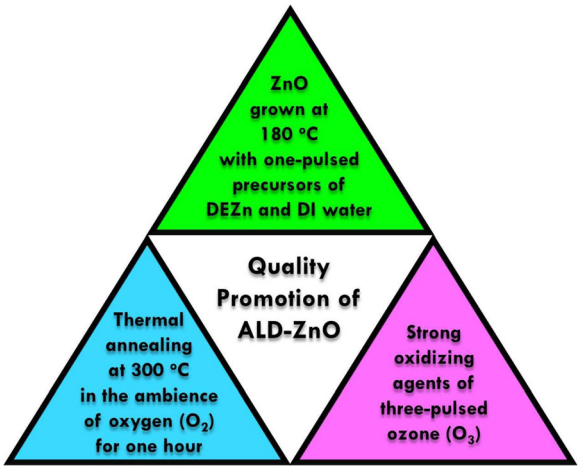

Fig. 6 A pyramid diagram. In the pyramid, four triangles are illustrated in different colors. Three triangles at the edges of the pyramid show key growth and processing conditions of ZnO. Combination of these three crucial components in the growth promotes quality of ALD ZnO epilayers shown by the triangle at the center of the pyramid

roughness. Post-deposition TA at 300 °C in the ambience of oxygen (O_2) for 1 h can further facilitate the formation of more defect-free grains with lower strain/stress, lower background electron concentration, and melioration of surface roughness after the growth of using three-pulsed O_3 precursors. The lowest strain/stress and background electron concentration which are 0.49%/2.22 GPa and 9.4×10^{15} cm^{-3}, respectively, owing to the dramatic decrease of intrinsic native defect of ALD-grown ZnO thin films are attained.

Abbreviations

ALD: Atomic layer deposition; O_3: Ozone; TA: Thermal annealing; O_2: Oxygen; PL: Photoluminescence; H_2O: Water; H_2O_2: Hydrogen peroxide; OH: Hydroxyl; Zn_i: Zinc interstitials; V_O: Oxygen vacancies; TDs: Threading dislocations; GBs: Grain boundaries; NBE: Near bandgap edge; c-Al_2O_3: c-face sapphire; DI: Deionized; C_2H_5: Ethyl groups; N_2: Nitrogen gas; Zn: Zinc; XRD: X-ray diffraction; AFM: Atomic force microscope; RMS: Root mean square

Acknowledgements

This work was correlated with Grant Proposal No. 107WFA0F10149 of Prof. Yung-Chen Cheng submitted to the Ministry of Science and Technology (MOST) and revised Grant Proposal supported by the National University of Tainan. It was also supported by MOST Grant Proposal No. 108-2823-8-194-002 of Prof. Hsiang-Chen Wang (National Chung Cheng University).

Authors' Contributions

YCC processed the experimental data, performed the analysis, drafted the manuscript, and designed the figures. HCW aided in interpreting the results. TPL, SKF, and KYY carried out the experiments and collected the data. YCC supervised the work of TPL. SWF supervised the work of SKF. MJC supervised the work of KYY. All authors read and approved the final manuscript.

Funding

This funding was supported by biomedical leap projects for cross-industry integration B10801 approved by Hsinchu Science Park of the Ministry of Science and Technology in Taiwan.

Availability of Data and Materials

The data that support the findings of this study are available from the corresponding author (Yung-Chen Cheng) upon reasonable request.

Competing Interests

The authors declare that they have no competing interests.

Author details

[1]Department of Materials Science, National University of Tainan, Tainan 70005, Taiwan. [2]Department of Mechanical Engineering and Advanced Institute of Manufacturing with High-tech Innovations, National Chung Cheng University, Chia Yi 62102, Taiwan. [3]Department of Applied Physics, National University of Kaohsiung, Kaohsiung 81148, Taiwan. [4]Department of Materials Science and Engineering, National Taiwan University, Taipei 10617, Taiwan.

Received: 13 October 2019 Accepted: 14 July 2020
Published online: 29 July 2020

References

1. Weckman T, Laasonen K (2016) Atomic layer deposition of zinc oxide: diethyl zinc reactions and surface saturation from first-principles. J Phys Chem C. 120:21460–21471
2. Wang Y, Kang K-M, Kim M, Park H-H (2018) Low temperature method to passivate oxygen vacancies in un-doped ZnO films using atomic layer deposition. Thin Solid Films. 660:852–858
3. Park J, Jung T-H, Lee J-H, Kim H-S, Park J-S (2015) The growth behavior and properties of atomic layer deposited zinc oxide films using hydrogen peroxide (H_2O_2) and ozone (O_3) oxidants. Ceram Int. 41:1839–1845
4. Janocha E, Pettenkofer C (2011) ALD of ZnO using diethylzinc as metal-precursor and oxygen as oxidizing agent. Appl Surf Sci. 257:10031–10035
5. Knoops HCM, Elam JW, Libera JA, Kessels WMM (2011) Surface loss in ozone-based atomic layer deposition processes. Chem Mater. 23:2381–2387
6. Kim H, Wang Z, Hedhili MN, Wehbe N, Alshareef HN (2017) Oxidant-dependent thermoelectric properties of undoped ZnO films by atomic layer deposition. Chem Mater. 29:2794–2802
7. George SM (2010) Atomic layer deposition: an overview. Chem Rev. 110: 111–131
8. Johnson RW, Hultqvist A, Bent SF (2014) A brief review of atomic layer deposition: from fundamentals to applications. Mater Today. 17:236–246
9. Tynell T, Karppinen M. Atomic layer deposition of ZnO: a review. Semicond Sci Technol. 2014;29:043001-1–043001-5.
10. McCluskey MD, Jokela SJ. Defects in ZnO. J Appl Phys. 2009;106:071101-1–071101-13.
11. Look DC, Hemsky JW, Sizelove JR (1999) Residual native shallow donor in ZnO. Phys Rev Lett. 82:2552–2555
12. Zhang SB, Wei S-H, Zunger A. Intrinsic n-type versus p-type doping asymmetry and the defect physics of ZnO. Phys Rev B. 2001;63:075205-1–075205-7.
13. Van de Walle CG (2000) Hydrogen as a cause of doping in zinc oxide. Phys Rev Lett. 85:1012–1015
14. Chichibu SF, Kojima K, Yamazaki Y, Furusawa K, Uedono A. Controlling the carrier lifetime of nearly threading-dislocation-free ZnO homoepitaxial films by 3d transition-metal doping. Appl Phys Lett. 2016;108:021904-1–021904-5.
15. Ellmer K, Mientus R (2008) Carrier transport in polycrystalline transparent conductive oxides: a comparative study of zinc oxide and indium oxide. Thin Solid Films. 516:4620–4627
16. McCluskey MD, Corolewski CD, Lv J, Tarun MC, Teklemichael ST, Walter ED, Norton MG, Harrison KW, Ha S. Acceptors in ZnO. J Appl Phys. 2015;117: 112802-1–112802-6.
17. Ozgur U, Hofstetter D, Morkoc H (2010) ZnO devices and applications: a review of current status and future prospects. Proc IEEE. 98:1255–1268
18. Vidya R, Ravindran P, Fjellvåg H, Svensson BG, Monakhov E, Ganchenkova M, Nieminen RM. Energetics of intrinsic defects and their complexes in ZnO investigated by density functional calculations. Phys Rev B. 2011;83:045206-1–045206-12.
19. Goyal A, Stevanovic V. Metastable rocksalt ZnO is p-type dopable. Phys Rev Materials. 2018;2:084603-1–084603-6.
20. Wu I-C, Weng Y-H, Lu M-Y, Jen C-P, Fedorov VE, Chen WC, Wu MT, Kuo C-T. Wang H-C. Nano-structure ZnO/Cu_2O photoelectrochemical and self-

powered biosensor for esophageal cancer cell detection. Opt Express. 2017; 25:7689–7706.
21. Chen Y-S, Liao C-H, Chueh Y-L, Lai C-C, Chen L-Y, Chu A-K, Kuo C-T, Wang H-C (2014) High performance Cu_2O/ZnO core-shell nanorod arrays synthesized using a nanoimprint GaN template by the hydrothermal growth technique. Opt Mater Express. 4:1473–1486
22. Ting S-Y, Chen P-J, Wang H-C, Liao C-H, Chang W-M, Hsieh Y-P, Yang CC (2012) Crystallinity improvement of ZnO thin film on different buffer layers grown by MBE. J Nanomater. 2012:1–7
23. Hur T-B, Hwang Y-H, Kim H-K. Strain effects in ZnO thin films and nanoparticles. J Appl Phys. 2006;99:064308-1–064308-5.
24. Rao TP, Santhosh Kumar MC, Angayarkanni SA, Ashok M (2009) Effect of stress on optical band gap of ZnO thin films with substrate temperature by spray pyrolysis. J Alloy Comp. 485:413–417
25. Chen H-C, Chen M-J, Wu M-K, Cheng Y-C, Tsai F-Y (2008) Low-threshold stimulated emission in ZnO thin films grown by atomic layer deposition. IEEE J Sel Top Quant Electron. 14:1053–1057
26. Cheng Y-C, Yuan K-Y, Chen M-J (2016) ZnO thin films prepared by atomic layer deposition at various temperatures from 100 to 180 °C with three-pulsed precursors in every growth cycle. J Alloy Comp. 685:391–394
27. Wang H-C, Liao C-H, Chueh Y-L, Lai C-C, Chou P-C, Ting S-Y (2013) Crystallinity improvement of ZnO thin film by hierarchical thermal annealing. Opt Mater Express. 3:295–306
28. Wang H-C, Liao C-H, Chueh Y-L, Lai C-C, Chen L-H, Tsiang R C-C. Synthesis and characterization of ZnO/ZnMgO multiple quantum wells by molecular beam epitaxy. Opt Mater Express. 2013;3: 237-247.
29. Cheng Y-C, Yuan K-Y, Chen M-J (2017) Influence of homo-buffer layers and post-deposition rapid thermal annealing upon atomic layer deposition grown ZnO at 100 °C with three-pulsed precursors per growth cycle. J Cryst Growth. 475:39–43

Publisher's Note